

Modelling and simulation of the curing process of polymers by a modified formulation of the Arruda–Boyce model

M. HOSSAIN, P. STEINMANN

Chair of Applied Mechanics

University of Erlangen-Nuremberg, Germany

e-mails: hossain@ltm.uni-erlangen.de, steinmann@ltm.uni-erlangen.de

A PHENOMENOLOGICALLY MOTIVATED SMALL STRAIN MODEL and a finite strain general framework to simulate the curing process of polymer have been developed and discussed in our recently published papers [1, 2, 3, 4]. In order to illustrate the capability of the finite strain framework proposed earlier, only the micromechanically-inspired 21-chain model and the phenomenologically motivated Neo-Hookean model (energy function) have been demonstrated so far. The Arruda–Boyce model (well-known as the 8-chain model in the elastic case and Bergström–Boyce model [5, 14] in the viscoelastic case) is a prototype hyperelastic model for polymeric materials. This follow-up contribution presents an extension of the Arruda–Boyce model [6] towards modelling the curing process of polymers. The necessary details, i.e. the stress tensor and the tangent operator, for the numerical implementation within the finite element method, are derived. The curing process of polymers is a complicated process where a series of chemical reactions have been activated, which will convert low molecular weight monomer solutions into more or less cross-linked solid macromolecular structures via the chemical conversion. This paper will model the elastic behaviour and shrinkage effects of the polymer curing process in the isothermal case using the Arruda–Boyce model. Several numerical examples have been demonstrated to verify our newly proposed, modified approach in case of curing process.

Key words: curing, polymer, finite strain, elasticity, Arruda–Boyce model.

Copyright © 2011 by IPPT PAN

1. Introduction

THERE ARE WIDE-RANGE APPLICATIONS of polymeric materials, especially for adhesives in household usages and in industrial sectors [12]. Normally, adhesive materials are used in the uncured stage (formation phase) in many cases, e.g. for adhesives in the automotive, electronics or aerospace industry. In order to predict different mechanical behaviours during curing, one can observe an increasing demand for constitutive models and simulation methods that consider a time or degree of cure dependence of the mechanical properties. The curing process is a phase transition process from the (viscous) liquid phase to the (viscoelastic) solid phase via chemical reactions, with the formation and crosslinking

of new polymer chains. Note that this transition process is modeled by the time-dependent material parameters in a continuum sense rather than modelling the chemical transformation of the underlying material structures.

A comprehensive and fair review on the small and large strain constitutive models for simulating the curing process of polymers has been discussed in HOSSAIN *et al.* [1, 2, 3]. Although several approaches can be found in the literature [24, 25] for modelling of the curing processes, but these efforts are mainly restricted to model residual stress build-up in polymer composites during curing. Kiasat developed a small-strain curing model for isothermal case after performing considerable illustrative experimental works. This simple model is based on the assumption of time-dependent material parameters within the framework of linear viscoelasticity. Additionally, he assumes that new cross-links form unstrained and stress-free, i.e. new cross-links will not carry any load applied earlier. Another excellent but complicated approach for polymer curing has been proposed by ADOLF and co-workers in a series of papers [10, 11, 12], in which they proposed both small-strain and finite strain constitutive models. Recently, LION and HÖFER [8] developed a phenomenologically-motivated thermo-viscoelastic coupled curing model for large strain curing. Later on, this model is used by the same research group in different practical applications, i.e. curing of bone-cement [9]. The modular structure of this model makes it attractive since it decomposes the deformation gradient into mechanical, thermal and chemical shrinkage parts, in order to account for thermally and chemically induced volume and temperature changes.

In the earlier proposed finite strain framework for curing, we only used the recently proposed 21-chain energy function from a group of micromechanical models. The 21-chain model, also known as micro-sphere model [20, 21, 22], is computationally costly since it requires loops over the 21-direction of a unit sphere at each Gauss-point level. Additionally, the viscoelastic part of the energy function of the 21-chain model is somehow phenomenologically motivated, i.e. there is no micromechanical explanation of its underlying material parameters. On the other hand, the Arruda–Boyce model is well-known in the polymeric material modelling community which is comparatively easy to compute and has already been implemented in some widely-used commercial softwares. Most interestingly, this model has a micromechanical explanation of its viscoelastic extension and evolution laws [5, 14]. The aim of this contribution is to apply the previously proposed finite strain framework to the Arruda–Boyce energy function and to extend it to the curing process of polymers in isothermal conditions. The necessary ingredients for the finite element implementation, i.e. a full derivation of stress tensor and consistent tangent operator, which are essential for the iterative solution of boundary value problems within a finite element scheme, have been derived.

The paper is organized as follows: In Section 2, the main algorithmic framework which was discussed in our previous papers are reproduced in a comprehensive way. Section 3, a short review on the Arruda–Boyce model and its detailed extension towards the curing process modelling are demonstrated. In Section 4, the modelling approach for the curing shrinkage via the multiplicative decomposition is described briefly. Section 5, the material parameters evolution during curing is discussed shortly. In Section 6, some illustrative numerical examples are presented to make our proposed model plausible. Finally, concluding remarks close the paper.

2. Curing simulation framework

A thermodynamically consistent general framework for finite strain elastic curing modelling in a rate-form (hypoelastic) was proposed in our previous publications [2, 3] as

$$(2.1) \quad \dot{\mathbf{S}}(t) = \frac{1}{2}\mathbb{C}(t) : \dot{\mathbf{C}}(t),$$

where \mathbf{S} and \mathbf{C} denote the second Piola–Kirchhoff stress tensor and the right Cauchy–Green strain tensor, respectively. In Eq. (2.1), $(\dot{\bullet})$ denotes the material time-derivative and $\mathbb{C}(t)$ describes the time-dependent stiffness operator as derived from the free energy density Ψ of an arbitrary hyperelastic constitutive model via

$$(2.2) \quad \mathbb{C} = 4 \frac{\partial^2 \Psi}{\partial \mathbf{C}^2}.$$

Note that in our model we allow \mathbb{C} to obey the time-dependent material parameters. This formulation can be shown to be thermodynamically consistent by introducing an energy function

$$\Phi(t) = \frac{1}{2} \int_0^t [\mathbb{C}'(s) : [\mathbf{E}(t) - \mathbf{E}(s)]] : [\mathbf{E}(t) - \mathbf{E}(s)] ds,$$

where $\mathbb{C}'(s) = d\mathbb{C}(s)/ds$ and \mathbf{E} is the Green–Lagrange strain tensor. The relation (2.1) is a tensor-valued, ordinary differential equation which can iteratively be solved by applying numerical integration schemes such as the trapezoidal method or the Euler backward method. By discretizing with the unconditionally stable implicit Euler backward scheme, it yields

$$(2.3) \quad \mathbf{S}^{n+1} = \mathbf{S}^n + \frac{1}{2}\mathbb{C}^{n+1} : [\mathbf{C}^{n+1} - \mathbf{C}^n].$$

In order to incorporate a constitutive model in the form suited for a finite element implementation, a consistent linearisation of the stress formulation (2.3) with respect to the strain is necessary. The computation of the current tangent operator introduces a sixth-order tensor, namely the derivative of the current material specific stiffness operator with respect to the strain as

$$(2.4) \quad \mathbb{E}^{n+1} = 2 \frac{\partial \mathbf{S}^{n+1}}{\partial \mathbf{C}^{n+1}} = \mathbb{C}^{n+1} + [\mathbf{C}^{n+1} - \mathbf{C}^n] : \mathfrak{A}^{n+1},$$

where $\mathfrak{A}^{n+1} = \partial \mathbf{C}^{n+1} / \partial \mathbf{C}^{n+1}$. In the following sections, the framework for the simulation of curing materials described above will be applied for the Arruda–Boyce hyperelastic model. From the free energy of the Arruda–Boyce model, the stiffness operator \mathbb{C} and the corresponding tangent operator \mathbb{E} are derived.

3. Arruda–Boyce base model

The Arruda–Boyce model [6, 19] is a classical and widely-used constitutive model using the Langevin chains statistics. The constitutive relation is based on an eight chains representation of the underlying macromolecular network structure, where the individual chains use the non-Gaussian behaviour for finite extensibility. This model accurately captures the network deformation up to the maximum level while requiring only two material parameters, shear modulus and number of segments per chain. Since these two material parameters have a micromechanical explanation which links the physics of molecular chain orientation involved in the deformation of rubber, the Arruda–Boyce model represents a simple and accurate constitutive model for finite deformation of polymeric materials. It is noted here that the unit volume element is assumed to have edges parallel to the principal isochoric directions which is composed of 8 chains oriented in the diagonal form (hence most-frequently the Arruda–Boyce model is termed as the 8-chain model) from the center of the volume to its corners, see Fig. 1.

If the chain conformation incorporates the non-Gaussian statistics for a random walk single chain, then the energy function φ_i of a particular chain consisting of N identical segments as has been introduced by KUHN and GRÜN [23], i.e.

$$(3.1) \quad \varphi(\lambda_r) = k\Theta N \left[\lambda_r \mathcal{L}^{-1}(\lambda_r) + \ln \frac{\mathcal{L}^{-1}(\lambda_r)}{\sinh \mathcal{L}^{-1}(\lambda_r)} \right],$$

where $\lambda_r = \lambda / \sqrt{N}$ denotes the relative chain stretch, k, Θ are Boltzmann's constant and absolute temperature, respectively, and $\mathcal{L}(\bullet) = \coth(\bullet) - 1/(\bullet)$ is the Langevin's function. There are several ways proposed in the literature [4, 21]

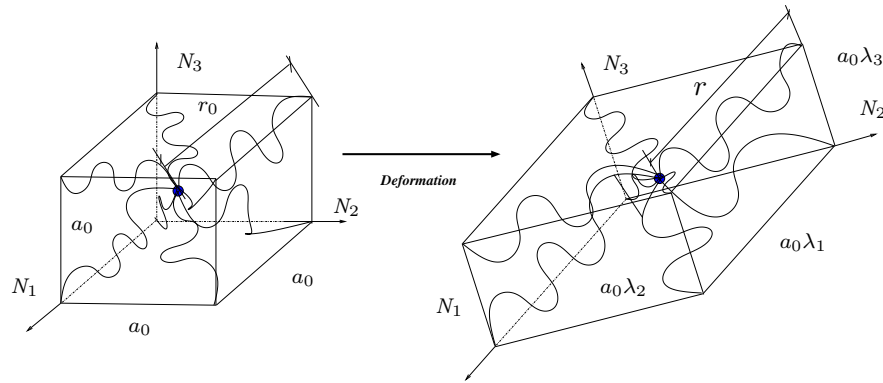


FIG. 1. Arruda–Boyce model: undeformed and deformed configurations.

to find the inversion of the Langevin function (one often uses \mathcal{L}^{-1} to denote it), the Pade approximation is one of them as

$$(3.2) \quad \gamma := \mathcal{L}^{-1}(\lambda_r) \approx \lambda_r \frac{3 - (\lambda_r)^2}{1 - (\lambda_r)^2}.$$

According to certain literature, e.g. [14, 16, 20], the Pade approximation has advantages over the polynomial approximations, i.e. it has a simple form which shows the singular behaviour of the inverse Langevin function at $\lambda_r = 1$ with good results. To obtain the macro-level free energy from the free energy of a single chain, the averaging should be performed via $\Psi(\mathbf{C}, J) = n \langle \varphi(\lambda_r) \rangle$; for details, see cf. LULEI [21]. Note that now the relative macro-stretch λ_r will be related to the right Cauchy–Green tensor via

$$\lambda_r = \sqrt{\frac{1}{3N} [\lambda_1^2 + \lambda_2^2 + \lambda_3^2]} = \sqrt{\frac{\text{tr} \mathbf{C}}{3N}},$$

where λ_i ($i = 1, 2, 3$) are the eigenvalues of the right Cauchy–Green tensor. Using the relation for the shear modulus as $\mu := nk\Theta$ and adding a penalty term as in the Neo–Hookean case, the free energy density of the 8-chain model finally reads

$$(3.3) \quad \Psi(\mathbf{C}, J) = \mu N \left[\gamma \lambda_r + \ln \frac{\gamma}{\sinh \gamma} \right] + \frac{1}{2} \kappa (\ln J)^2 - \mu \ln J,$$

where κ is the compression modulus. Subsequently, the curing simulation framework requires the computation of the current stiffness and tangent operator. Application of Eq. (2.2) to (3.3) yields

$$(3.4) \quad \mathbb{C}^{n+1} = 4 \frac{\partial^2 \Psi}{\partial \mathbf{C}^2} = \frac{4\mu^{n+1} N^{n+1}}{9N^{n+1} [1 - \lambda_r^2]^2} [\mathbf{I} \otimes \mathbf{I}] + \kappa^{n+1} \mathbb{A} - 2 [\mu^{n+1} - \kappa^{n+1} \ln J] \mathbb{B},$$

where N^{n+1} , κ^{n+1} and μ^{n+1} are cure-dependent material parameters termed as the number of segments per chain, the bulk and shear moduli, respectively. The second order identity tensor \mathbf{I} is defined as $\mathbf{I} = \delta_{ij} \mathbf{e}_i \otimes \mathbf{e}_j$, δ_{ij} being the Kronecker delta. For a detailed derivation, the reader is referred to e.g. [4, 17, 18]. The fourth-order tensors \mathbb{A} and \mathbb{B} appearing in Eq. (3.4) can be written in indicial notation as in the Appendix. Another partial derivative with respect to \mathbf{C} yields the sixth-order tensor which is also a part of the current tangent operator for the Arruda–Boyce elastic curing model

$$(3.5) \quad \begin{aligned} \mathfrak{A}^{n+1} &= \frac{\partial \mathbf{C}^{n+1}}{\partial \mathbf{C}} \\ &= \frac{8\mu^{n+1}N^{n+1}}{27N^{2,n+1}[1 - \lambda_r^2]^3} [\mathbf{I} \otimes \mathbf{I} \otimes \mathbf{I}] \\ &\quad + \kappa^{n+1} [\mathfrak{B} + 2 \ln J \mathfrak{C} + \mathbb{B} \otimes \mathbf{C}^{-1}] - 2\mu^{n+1} \mathfrak{C}, \end{aligned}$$

with the abbreviations \mathfrak{B} , \mathfrak{C} as defined in the Appendix and also in Section 4 of [2]. Up to this section, all necessary ingredients required for the Arruda–Boyce elastic curing model are ready.

4. Modelling curing shrinkage

The curing shrinkage is one of the most important pathological phenomena observed during polymer curing, which means the reduction of the specific volume due to chain growth and/or cross-linking that may show significant residual stresses and/or strains in case of specimen held within fixed boundaries during curing. Two distinct approaches to incorporate the shrinkage effect into constitutive models have been proposed and discussed in details in our earlier papers [2, 3], i.e.: (1) the superposition of an exponentially decaying shrinkage strain function, which has been proposed and demonstrated by KIASAT [13], and (2) a multiplicative decomposition of the deformation gradient, advocated by LION and HÖFER [8]. One curing shrinkage approach will be recapitulated briefly in order to apply it in case of Arruda–Boyce curing model. The application of a multiplicative decomposition of the deformation gradient is frequently used in viscoelasticity and in viscoplasticity, but within the context of curing shrinkage has been first suggested by LION and HÖFER [8]. Decomposing the deformation gradient into two parts, i.e. a stress producing mechanical part and a volume reducing shrinkage part yields

$$(4.1) \quad \mathbf{F} = \mathbf{F}_m \cdot \mathbf{F}_s \quad \text{with} \quad \mathbf{F}_s = [1 + \alpha s]^{1/3} \mathbf{I}.$$

Therein, $\alpha \in [0, 1]$ denotes the degree of cure, cf. [1], and $s \leq 0$ is an user-defined parameter controlling the magnitude of the shrinkage. From the usual thermo-

dynamical argumentation, the corresponding second Piola-Kirchhoff stress is obtained

$$(4.2) \quad \mathbf{S} = [1 + \alpha s]^{-2/3} \mathbf{S}_m,$$

with the mechanical stress \mathbf{S}_m . The necessary tangent operator is again obtained by linearising the stress with respect to the strain for which the chain rule yields

$$(4.3) \quad \mathbb{E} = [1 + \alpha s]^{-4/3} \mathbb{E}_m,$$

with $\mathbb{E}_m = 2\partial\mathbf{S}_m/\partial\mathbf{C}_m$ denoting the mechanical tangent operator that has to be calculated. Both Eqs. (4.2) and (4.3) show that without application of external (mechanical) load, stress will be generated due to the chemical shrinkage.

5. Material parameters evolution

The temporal evolution of the material parameters during curing has been demonstrated in our previous papers [1, 2] and also in DAL and KALISKE [7], where a simple expression describing such a behaviour for the shear modulus is

$$(5.1) \quad \mu(t) = \mu_0 + [\mu_\infty - \mu_0][1 - \exp(-\kappa_\mu t)],$$

whereas the initial and final values μ_0 and μ_∞ , as well as the curvature parameter κ_μ , are required. Maintaining the mass conservation principal, the current number of chain segments in a single chain can be calculated in the way following,

$$n(t)N(t) = n_0N_0 \Rightarrow N(t) = \frac{\mu_0 N_0}{\mu(t)},$$

i.e. if the initial values of μ_0 and N_0 are prescribed, the evolution of $\mu(t)$ will provide the current value for the number of chain segments, $N(t)$.

6. Numerical examples

In this section, several numerical examples are presented to demonstrate that the proposed extension of the Arruda-Boyce model to the case of curing simulation, can reproduce the typical mechanical behaviour during isothermal curing. In an attempt to verify the extension, two benchmark simulations are presented which were also discussed in our earlier publications [2] with different energy functions, i.e. a gain in stiffness and a stress rate of zero in case when the strain rate becomes zero. Initially, one one-dimensional example which reflects the behaviour of a single eight-noded brick element with a prescribed uniaxial stretch history and parameter evolution are presented, see Fig. 2. Later on, two three-dimensional examples are presented, i.e. a plate with a centered hole (symmetric half-part) is studied to demonstrate the fact that the material be-

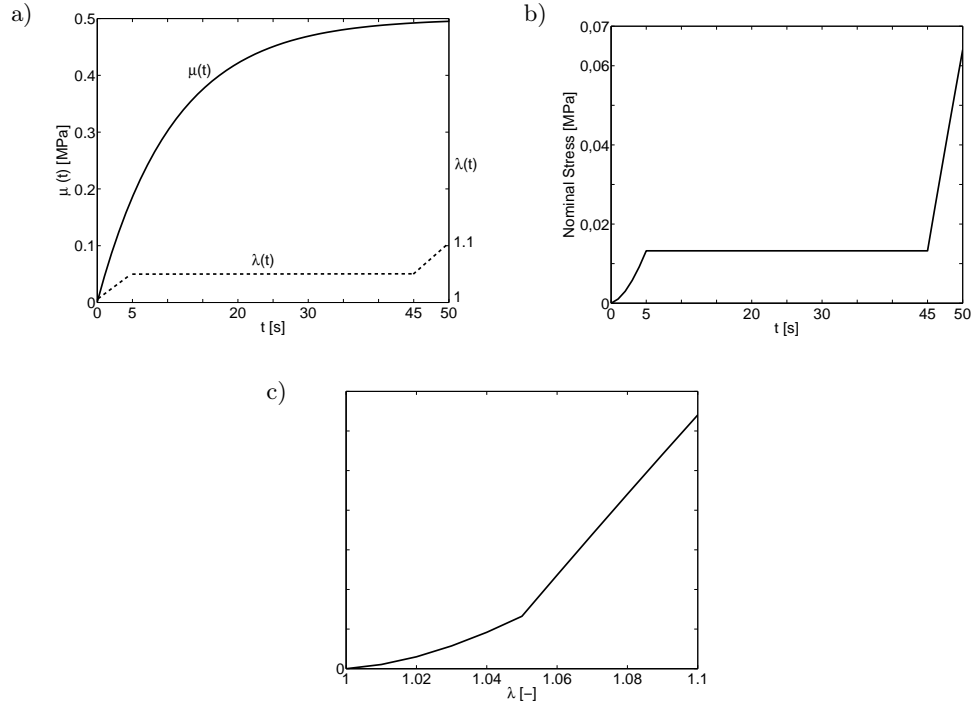


Fig. 2. a) Evolution of shear modulus $\mu(t)$ as in Eq. (5.1) where $[\mu_0, \mu_\infty, \kappa_\mu, N_0] = [0.001 \text{ MPa}, 0.5 \text{ MPa}, 0.0925 \text{ s}^{-1}, 10^4]$ and applied load history $\lambda(t)$ to the Arruda-Boyce elastic curing model. b) First Piola stress vs. time. c) First Piola stress vs. stretch.

comes stiffer during a curing process, and another example is presented to show the shrinkage-induced stress development if the specimen is held within fixed boundaries during curing. In order to avoid more complexity, the bulk modulus evolution has always been calculated from the current shear modulus via

$$\kappa(t) = \frac{2\mu(t)}{3} [1 + \nu][1 - \nu]^{-1}.$$

Due to lack of sufficient experimental data for the evolution of Poisson's ratio during curing, we follow O'BRIEN *et al.* [24] assumption of a constant ν , e.g. $\nu = 0.35$.

6.1. One-dimensional example

In order to substantiate whether the proposed extension of the Arruda-Boyce model reproduces the central assumption upon which the finite strain curing framework is based, i.e. the gain in stiffness during the advancement of curing and no stress-increment in case the strain rate becomes zero, a simple one-dimensional uniaxial tension test using a single finite element is presented here.

In this simulation, a three-phase deformation, i.e. pull-hold-pull, is applied consisting of a linear increase to $\lambda = 1.05$ (continuum/macroscopic stretch) within the first five seconds, which is followed by forty seconds holding and another linear increase to $\lambda = 1.1$ during the last five seconds, cf. Fig. 2a. Following the temporal evolving nature of the shear modulus during curing as presented in the literature [13], the simplest possible form, i.e. an exponential saturation function as depicted in Fig. 2a, is used in the simulation. The resulting stress responses versus time and stretch are given in Figs. 2b and 2c. The main assumption that is considered during our model development, i.e. the stiffness increase during curing has no impact on the stress response of a constant deformation state, is correctly reproduced, which is reflected by the constant lines between 5 and 45 seconds (Fig. 2b) and, implicitly, by the kinks at $\lambda = 1.05$ that stem from the continuous increase of μ (Fig. 2c).

6.2. Three-dimensional examples

To demonstrate the stiffness gain due to curing, a three-dimensional plate with a hole in its center is considered. This example represents a typical boundary value problem with inhomogeneous stress distribution under load. Its dimensions are $60 \times 12 \times 2 \text{ mm}^3$ and the hole has a diameter of 6 mm. The plate is discretised by 544 eight-noded hexagonal elements and is supported as depicted in Fig. 3a. Due to symmetry boundary conditions, only one half of the geometry has been

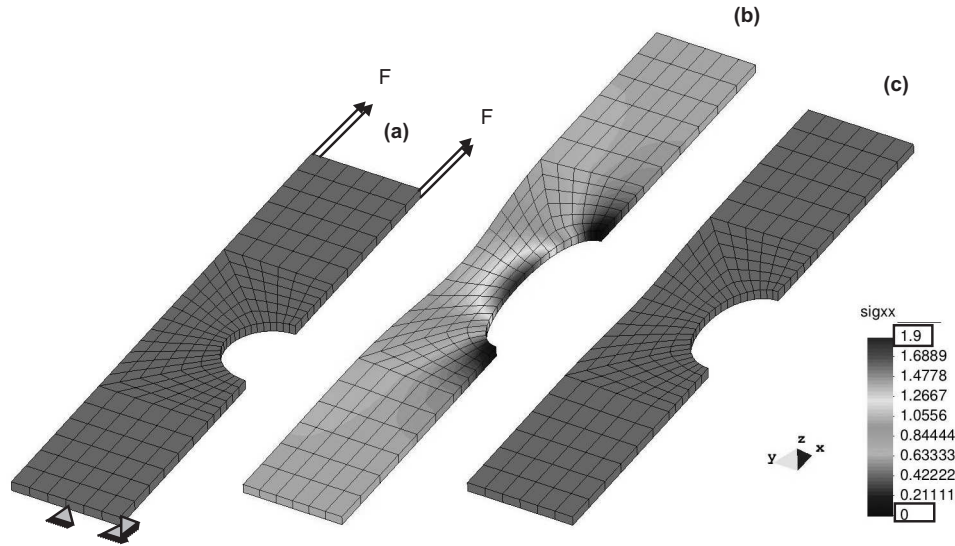


Fig. 3. Demonstration of stiffness gain: inhomogeneous 3D-example, Arruda–Boyce elastic curing model; a) initial configuration, boundary conditions and loading; b) deformation and Cauchy stress after ten loadsteps $\Delta F_x = 0.6 \text{ N}$; c) stress-free but still deformed (due to stiffness gain) after ten reverse loadsteps $\Delta F_x = -0.6 \text{ N}$.

taken into consideration. Force increments of $0.6 N$ are applied at the upper edge to achieve elongations in the x -direction. While being loaded, the specimen undergoes elastic curing, whereas

$$[\mu_0, \mu_\infty, \kappa_\mu, N_0] = [0.0001 \text{ MPa}, 1.5 \text{ MPa}, 0.5 \text{ s}^{-1}, 1 \cdot 10^5].$$

Figures 3b and 3c depict the resulting deformations and Cauchy stresses in x -direction after ten tensile and another ten compressive loadsteps. First, tensile stresses and a significant deformation arise, cf. Fig. 3b, while after the second ten loadsteps of equal magnitude but reverse direction, the plate is stress-free but, due to the interim stiffness increase, still deformed, cf. Fig. 3c.

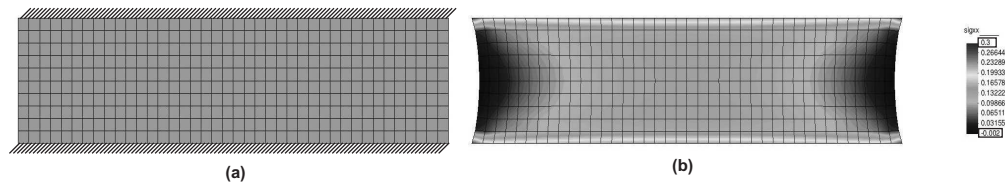


Fig. 4. a) Curing shrinkage of a three-dimensional thin-plate subjected to fixed boundary conditions; b) deformed shape and (Cauchy) stress in x -direction after 20s of curing. Arruda–Boyce model extended by multiplicative deformation approach of Sec. 4. Parameters used are:

$$[\mu_0, \mu_\infty, \kappa_\mu, s, N_0] = [0.0001 \text{ MPa}, 1.5 \text{ MPa}, 0.25 \text{ s}^{-1}, -0.1, 2 \cdot 10^6].$$

As we had discussed earlier, curing shrinkage is another important phenomenon which is nicely captured by the above-mentioned model. To prove the correct behaviour of our curing models for real three-dimensional structures, we consider an inhomogeneous thin-plate example which has dimensions of $40 \times 10 \times 0.5 \text{ mm}^3$ and being discretised by eight hundred eight-noded hex elements as depicted in Fig. 4a, cf. [15]. The parameter set used here is

$$[\mu_0, \mu_\infty, \kappa_\mu, s, N_0] = [0.0001 \text{ MPa}, 1.5 \text{ MPa}, 0.25 \text{ s}^{-1}, -0.1, 2 \cdot 10^6].$$

Boundary condition and loading are applied as depicted in Fig. 4a, i.e. upper and lower parts are fixed, the two short parts are free to move. It is evident from Fig. 4b that without application of external (mechanical) load, a substantial amount of residual stress and strains are generated due to curing shrinkage of ten percent ($s = -0.1$).

7. Conclusion

In this contribution, an extension of the Arruda–Boyce model for the modelling of curing processes has been proposed with all necessary ingredients, i.e. the stress update and tangent operator required for finite element implementation. Although, the main three-dimensional framework for the simulation of

polymeric materials undergoing finite strain curing processes has been developed earlier, this new extension will help those who are more familiar with the Arruda–Boyce constitutive model. The numerical examples demonstrate that the extended approach is suitable to correctly reproduce the relevant phenomena observable in curing polymers. Moreover, two important aspects of curing process, i.e. the extension towards viscoelastic and temperature effects are going to be dealt with in a future work.

8. Appendix

Various fourth and sixth-order tensors, i.e. \mathbb{A} , \mathbb{B} , \mathfrak{B} , \mathfrak{C} appearing in Eqs. (3.4) and (3.5), are defined as

$$(8.1) \quad (\mathbb{A})_{ijkl} = (\mathbf{C}^{-1} \otimes \mathbf{C}^{-1})_{ijkl} = C_{ij}^{-1} C_{kl}^{-1},$$

$$(8.2) \quad (\mathbb{B})_{ijkl} = \left(\frac{\partial \mathbf{C}^{-1}}{\partial \mathbf{C}} \right)_{ijkl} = -\frac{1}{2} \left[C_{ik}^{-1} C_{jl}^{-1} + C_{il}^{-1} C_{jk}^{-1} \right],$$

$$(8.3) \quad (\mathfrak{B})_{ijklpq} = \frac{\partial (C_{ij}^{-1} C_{kl}^{-1})}{\partial C_{pq}} = \frac{\partial C_{ij}^{-1}}{\partial C_{pq}} C_{kl}^{-1} + C_{ij}^{-1} \frac{\partial C_{kl}^{-1}}{\partial C_{pq}}$$

$$= -\frac{1}{2} \left[C_{ip}^{-1} C_{jq}^{-1} C_{kl}^{-1} + C_{iq}^{-1} C_{jp}^{-1} C_{kl}^{-1} \right. \\ \left. + C_{ij}^{-1} C_{kp}^{-1} C_{lq}^{-1} + C_{ij}^{-1} C_{kq}^{-1} C_{lp}^{-1} \right],$$

$$(8.4) \quad (\mathfrak{C})_{ijklpq} = -\frac{1}{2} \frac{\partial (C_{ik}^{-1} C_{jl}^{-1} + C_{il}^{-1} C_{jk}^{-1})}{\partial C_{pq}}$$

$$= \frac{1}{4} \left[C_{ip}^{-1} C_{kq}^{-1} C_{jl}^{-1} + C_{iq}^{-1} C_{kp}^{-1} C_{jl}^{-1} \right. \\ \left. + C_{ik}^{-1} C_{jp}^{-1} C_{lq}^{-1} + C_{ik}^{-1} C_{jq}^{-1} C_{lp}^{-1} \right. \\ \left. + C_{ip}^{-1} C_{lq}^{-1} C_{jk}^{-1} + C_{iq}^{-1} C_{lp}^{-1} C_{jk}^{-1} \right. \\ \left. + C_{il}^{-1} C_{jp}^{-1} C_{kq}^{-1} + C_{il}^{-1} C_{jq}^{-1} C_{kp}^{-1} \right].$$

References

1. M. HOSSAIN, G. POSSART, P. STEINMANN, *A small-strain model to simulate the curing of thermosets*, Computational Mechanics, **43**, 6, 769–779, 2009.
2. M. HOSSAIN, G. POSSART, P. STEINMANN, *A finite strain framework for the simulation of polymer curing. Part-I: Elasticity*, Computational Mechanics, **44**, 621–630, 2009.

3. M. HOSSAIN, G. POSSART, P. STEINMANN, *A finite strain framework for the simulation of polymer curing. Part-II: Viscoelasticity and shrinkage*, Computational Mechanics, **45**, 1, 210–129, 2010.
4. M. HOSSAIN, *Modelling and computation of polymer curing*, Dissertation, University of Erlangen-Nuremberg, Germany, 2010.
5. J.S. BERGSTRÖM, M.C. BOYCE, *Constitutive Modeling of the large strain time-dependent behaviour of elastomers*, Journal of Mechanics and Physics of Solids, **46**, 931–954, 1998.
6. E.M. ARRUDA, M.C. BOYCE, *A three-dimensional constitutive model for the large stretch behaviour of rubber elastic materials*, Journal of Mechanics and Physics of Solids, **41**, 389–412, 1993.
7. H. DAL, M. KALISKE, *Bergström–Boyce model for nonlinear finite rubber viscoelasticity: theoretical aspects and algorithmic treatment for the FE method*, Computational Mechanics, **44**, 6, 809–823, 2010.
8. A. LION, P. HÖFER, *On the phenomenological representation of curing phenomena in continuum mechanics*, Archives of Mechanics, **59**, 59–89, 2007.
9. A. LION, B. YAGIMLI, G. BAROUD, U. GOERKE, *Constitutive modelling of PMMA-based bone cement: a functional model of viscoelasticity and its approximation for time domain investigations*, Archives of Mechanics, **60**, 3, 221–242, 2008.
10. D.B. ADOLF, J.E. MARTIN, *Calculation of stresses in cross-linking polymers*, Journal of Composite Materials, **30**, 13–34, 1996.
11. D.B. ADOLF, J.E. MARTIN, R.S. CHAMBERS, S.N. BURCHETT, T.R. GUESS, *Stresses during thermoset cure*, Journal of Material Research, **13**, 530–550, 1998.
12. D.B. ADOLF, R.S. CHAMBERS, *A thermodynamically consistent, nonlinear viscoelastic approach for modelling thermosets during cure*, Journal of Rheology, **51**, 23–50, 2007.
13. M. KIASAT, *Curing shrinkage and residual stresses in viscoelastic thermosetting resins and composites*, PhD Thesis, TU Delft, The Netherlands, 2000.
14. H. DAL, M. KALISKE, *A micro-continuum-mechanical material model for failure of rubber-like materials: Application to ageing-induced fracturing*, Journal of Mechanics and Physics of Solids, **57**, 8, 1340–1356, 2009.
15. J. RETKA, P. HÖFER, *Numerische Simulation aushärtender Klebstoffe*, Diploma Thesis, Universität der Bundeswehr München, 2007.
16. J. DIANI, P. GILORMINI, *Combining the logarithmic strain and the full-network model for a better understanding of the hyperelastic behaviour of rubber-like materials*, Journal of the Mechanics and Physics of Solids, **53**, 2579–2596, 2005.
17. J. BONET, R.D. WOOD, *Nonlinear Continuum Mechanics for Finite Element Analysis*, Cambridge University Press, 1997.
18. P. WRIGGERS, *Nonlinear Finite Element Methods*. Springer, Berlin 2008.
19. M.C. BOYCE, E.M. ARRUDA, *Constitutive models of rubber elasticity: a review*, Rubber Chemistry and Technology, **73**, 504–523, 2000.
20. C. MIEHE, S. GÖKTEPE, F. LULEI, *A micro-macro approach to rubber-like materials: Part-I. The non-affine micro-sphere model of rubber elasticity*, Journal of the Mechanics and Physics of Solids, **52**, 2617–2660, 2004.

21. F. LULEI, *Mikromechanisch motivierte Modelle zur Beschreibung finiter Deformationen gummiartiger Polymere: Physikalische Modellbildung und Numerische Simulation*, PhD Thesis, Institut für Mechanik (Bauwesen), University of Stuttgart, 2002.
22. S. GÖKTEPE, *Micro-macro approaches to rubbery and glassy polymers: Predictive micromechanically-based models and simulations*, PhD Thesis, Institut für Mechanik (Bauwesen), University of Stuttgart, 2007.
23. W. KUHN, F. GRÜN, *Beziehungen zwischen elastischen Konstanten und Dehnungsdoppelbrechung hochelastischer Stoffe*, *Kolloid-Zeitschrift*, **101**, 248–271, 1942.
24. D.J. O'BRIEN, P.T. MATHER, S.R. WHITE, *Viscoelastic properties of an epoxy resin during cure*, *Journal of Composite Materials*, **35**, 883–904, 2001.
25. S.R. WHITE, H.T. HAHN, *Process modeling of composite materials: residual stress development during cure. Part I. Model formulation*, *Journal of Composite Materials*, **26**, 2402–2422, 1992.

Received May 3, 2011; revised version October 6, 2011.
